Materials Transactions, Vol. 50, No. 2 (2009) pp. 293 to 298

Electric Flame-Off Characteristics and Fracture Properties of 20 μm Thin Copper Bonding Wire

Fei-Yi Hung[1,*], Truan-Sheng Lui[2,*], Li-Hui Chen[2] and Yi-Chang Lin[2]

[1]*Institute of Nanotechnology and Microsystems Engineering, Center for Micro/Nano Science and Technology, National Cheng Kung University, Tainan, Taiwan 701, R.O.China*
[2]*Department of Materials Science and Engineering, National Cheng Kung University, Tainan, Taiwan 701, R.O.China*

In the present study, the neck fracture properties of annealed wire with $\phi = 20\,\mu m$ (0.8 mil) at 225°C for 1 hour and un-annealed wire were compared. In addition, the microstructural characteristics, the mechanical properties and the texture transition using EBSD methods before and after an electric flame-off (EFO) process were also studied. Experimental results indicate that the recrystallization temperature of the as-drawn wire was ~225°C, and the annealed copper wires possessed a fully annealed structure. Through recrystallization, the matrix structure transferred from long, thin grains to equiaxed grains and a few annealed twins. The microstructure of the free air ball (FAB) after an EFO process consisted of column-like grains, and grew from the heat-affected zone (HAZ) to the Cu ball. For the annealed and un-annealed wires, their preferred orientations on the wire and the neck were ⟨100⟩ // AD. Under the thermal effect of EFO, the orientation of the Cu balls were mainly ⟨101⟩ // AD and ⟨111⟩ // AD for annealed wires. Additionally, the hardness of the Cu balls and the strength of the neck sites of the EFO wires were able to affect the reliability of the copper wire bonding. [doi:10.2320/matertrans.MRA2008145]

(Received April 28, 2008; Accepted November 5, 2008; Published January 25, 2009)

Keywords: *wire bonding, electric flame-off (EFO), tensile property, electron backscatter diffraction (EBSD)*

1. Introduction

Thermosonic ball bonding is one of the preferred processes of electronic packaging to connect a semiconductor chip and a lead frame by a thin metal wire. Gold wire and copper wire are the preferred interconnection materials to bond with the aluminum metalized wafer pads during this process.[1,2] Gold is expensive, and the electrical conductivity and thermal conductivity of gold is lower than those of copper.[3,4] In addition, the inherent properties of higher tensile strength, hardness and stiffness of copper as well as its cost effectiveness compared to gold, have made it a preferred alternative.[3,5]

In general, three factors affect the reliability of copper wire bonding[3,6] namely: (1) Oxidation causes unusual bonding, (2) The lower strength of the annealed wire results in breakage, (3) The high hardness of copper wire can damage chips during the wire compressing process. As-drawn copper wire possesses higher strength and hardness, however its lower ductility reduces the reliability of bonding. So, the annealing treatment of as-drawn copper wire is very important. Many studies[2,3,6] have discussed the process variables such as bonding force, temperature and electric flame-off (EFO), etc. However, the recrystallization effect in the microstructure and the relevant mechanical properties of thin copper wires ($\phi = 20\,\mu m$) have still not been examined. In addition, because the breakage sites of electric flame-off (EFO) wires are in the neck between HAZ and the ball, it's clear that the breakage results from the structure of the neck zones and stress affecting the breakage sites.[2,6–10] Thus, this paper not only investigated the mechanical properties of un-annealed and annealed copper wires (at 225°C for 1 hour), but also investigated the crystallographic texture of the free air ball (FAB), the neck zones and heat-affected zones (HAZ) using electron back scatter diffraction (EBSD).

*Corresponding author, E-mail: fyhung@mail.mse.ncku.edu.tw: z7408020@email.ncku.edu.tw

2. Experimental Procedure

2.1 Annealing treatment and electric flame-off process

A copper ingot of 99.99% purity was drawn to thin copper wire with diameter $\phi = 20\,\mu m$ (ICP analysis of the chemical composition is shown in Table 1). 225°C was chosen for the vacuum (10^{-3} Pa) annealing for the as-drawn wire. The annealing time for the as-drawn wires was fixed at 1 hour, and followed by air cooling to room temperature. The melting of the wire tip was controlled by EFO process using a thermosonic wire bonder machine. To prevent oxidation during the ball-formation process, a 95% nitrogen-5% hydrogen gas mixture was maintained at a flow rate of $1\,L \cdot min^{-1}$.

2.2 Micro-hardness analysis and tensile testing

Micro-hardness measurements were performed on a cross section of the un-EFO copper wire, the ball and the HAZ after EFO process. The force was 5 g and the holding time was 10 sec. A schematic illustration (include EFO wire) of the hardness testing is shown in Fig. 1.

To understand the effect of annealing on the neck fracture property of the Cu wire, both the annealed and un-annealed wires were subjected to neck tensile testing, after which the relation between the characteristics of HAZ and recrystallization was investigated. The testing method used a plate clamp to fix the free air ball (FAB), while the wire tip was

Table 1 ICP analysis of the chemical composition of Cu wire (ppm).

Si	Fe	Mn	Ni	Zn	Ti	Pb	Sn	Cu
0.45	0.05	0.22	0.08	0.10	0.06	0.53	0.07	Bal.

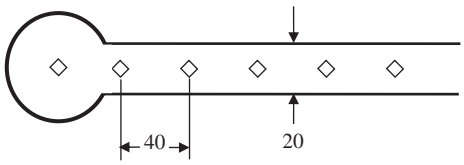

Fig. 1 The schematic illustration of the micro-hardness measuring. (unit: μm)

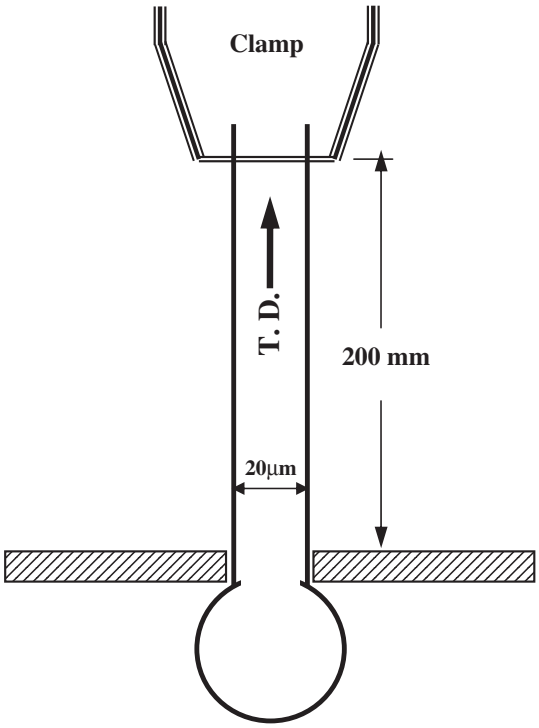

Fig. 2 The schematic illustration of the tensile testing for the neck.

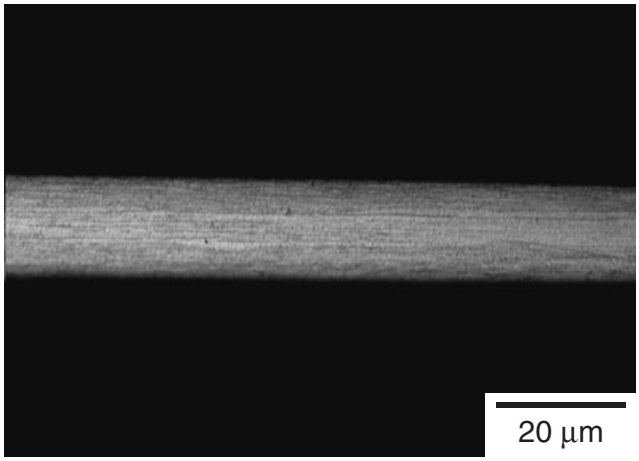

(a)

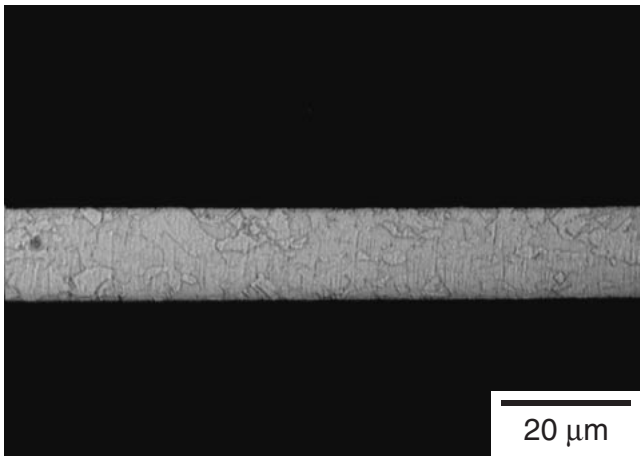

(b)

Fig. 3 Microstructures of the Cu wires: (a) as-drawn (un-annealed) and (e) annealed at 225°C for 1 hour.

fixed using a tongs-like clamp. A schematic illustration of the tensile test is shown in Fig. 2. The copper wire had a diameter of $\phi = 20\,\mu m$ and length of 200 mm. In addition, the tensile test results of each wire had a constant strain rate of $2.54\,cm{\cdot}min^{-1}$. With an aim to understand the tensile deformation mechanism of the wires and the Cu balls, the tensile fracture characteristics were observed using SEM. For tensile and hardness testing, each analysis datum is the average of 7 test results.

2.3 EBSD measurement

The bonding wires, including the free air ball (FAB), the neck zones and HAZ zones, were cut with a Focus Ion Beam (FIB) to prepare the electron back scatter diffraction (EBSD) specimens.[9,11,12] The orientations of the grains are shown in inverse pole figure (IPF) maps to obtain the texture information. For IPF maps, there are many points (>30 data) in the same specimen.

3. Results and Discussion

3.1 Microstructure and mechanical properties

The cross section microstructures of the annealed and un-annealed wires are shown in Fig. 3. The structure of the un-annealed wires contained long, thin grains parallel to the direction of drawing (see Fig. 3(a)). Figure 3(b) shows the structure of the 225°C annealed wire, revealing the copper wires contained fully annealed equiaxed grains and a few annealed twins. According to our previous data at an even higher annealing temperature, the matrix of the 250°C, 275°C and 300°C wires were still similar to those of the 225°C annealed wire. Notably, the 225°C annealed wire possessed a fully annealed structure and higher ductility. It can be inferred from what has been said above that a temperature of ~225°C is probably the recrystallization temperature of the as-drawn wire. The 225°C annealed wire was given EFO process and its data was compared with that of the un-annealed wires.

To investigate further, micro-hardness was measured (see Fig. 1) on the cross section of the copper wires before and after EFO process, as shown in Fig. 4. The results show that the hardness of the annealed wires had reduced significantly compared with the un-annealed wire. Additionally, micro-hardness analysis of the un-annealed wire and the 225°C annealed wire after EFO revealed that the neck of the FAB (i.e., HAZ) had the lowest value (see Fig. 4). Also, it can be seen from Fig. 4 that the hardness had a tendency to increase

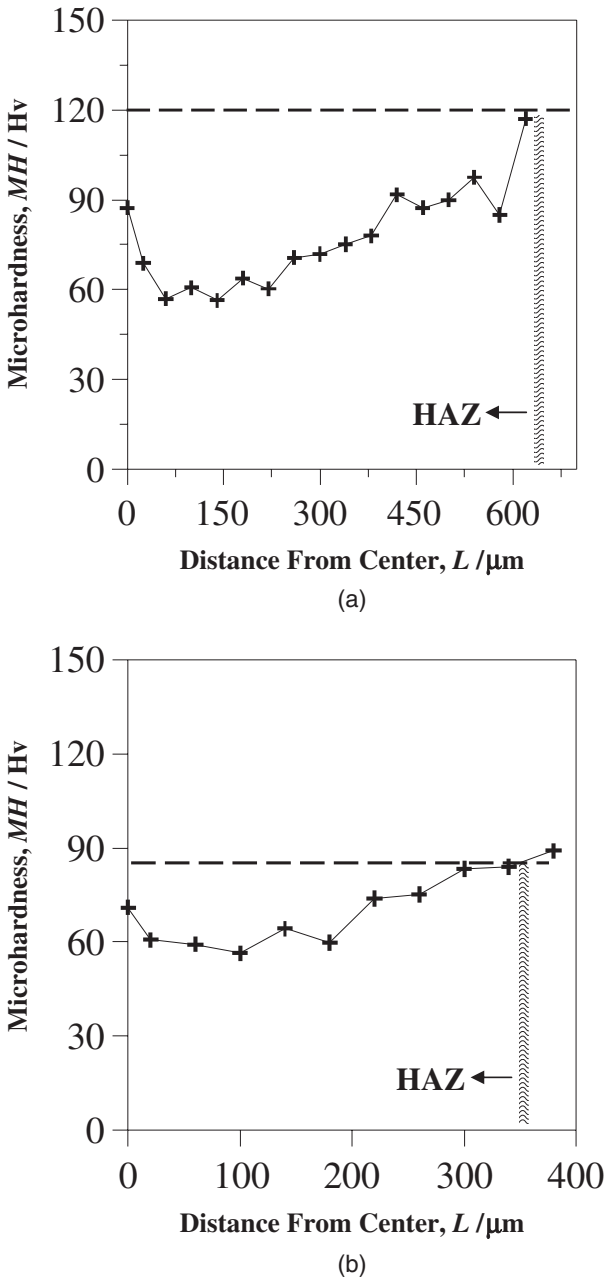

Fig. 4 Micro-hardness of the wire after EFO process (the origin of the cross axle is the center of FAB): (a) un-annealed wire and (b) 225°C annealed (The dotted line is the average hardness value of the un-EFO wires).

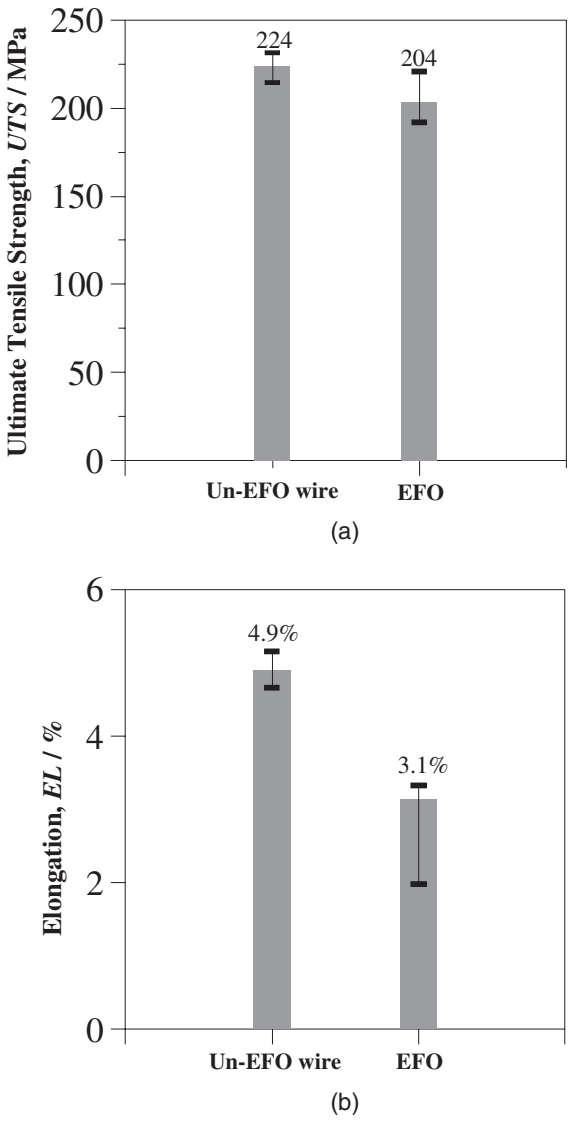

Fig. 5 Tensile mechanical properties of the 225°C annealed wire before and after EFO process: (a) UTS and (b) EL.

when this zone was far away from the Cu ball (origin of the *X*-axis). Comparing the data of Fig. 4(a) with Fig. 4(b), the HAZ of the annealed wire had a length of about 350 μm which was less than the un-annealed wire.

Figure 5 shows a comparison of the tensile test results of the 225°C annealed wires before and after EFO process (see Fig. 2, to measure the neck-strength and the breakage site). Regardless of the neck strength or elongation, the EFO process made the value lower than that of the without-EFO wires. This shows (1) the thermal effect from EFO process caused the grain growth, (2) the concentrated-stress on the neck near the ball caused a reduction in the tensile mechanical properties. Notably, the breakage site of the EFO wires were at the back of the neck, not at the back of the ball (see Fig. 6), revealing that structural variations from the EFO process affected the deformation resistance of the neck zone. Observing Fig. 4 and Fig. 6, we find that the breakage site of the EFO wires is probably in the heat-affected zone (HAZ). In addition, Fig. 6 shows a comparison of deformable capacity for the two Cu balls, revealing that the ductility of the Cu ball of the annealed wire was better than the un-annealed wire. Clearly, the hardness of the Cu ball with annealed wire was lower, and this result is similar to those in Fig. 4. Decreasing the hardness of the Cu ball is certainly one method to avoid damaging chips during the wire compressing process.[13,14)]

3.2 Crystallographic texture of Cu bonding wires

The microstructure (using ion beam etching) of the FAB of the annealed wire is shown in Fig. 7(a). The structure contained isotropic column-like grains, while the grains of the neck had grain growth induced by the heat of EFO process. Three positions, wires, FABs and necks of the

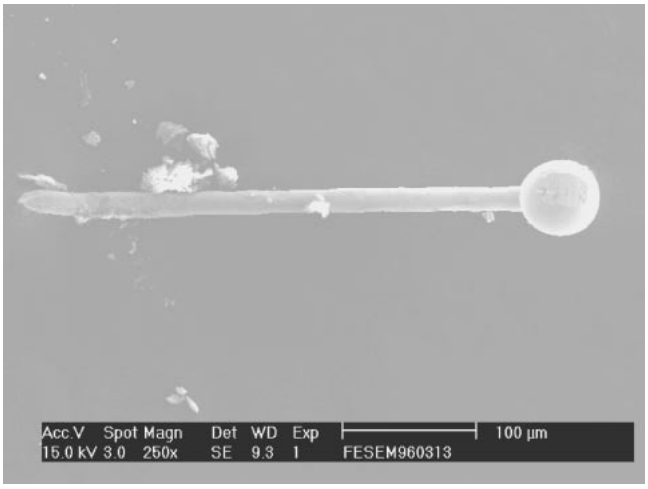

(a)

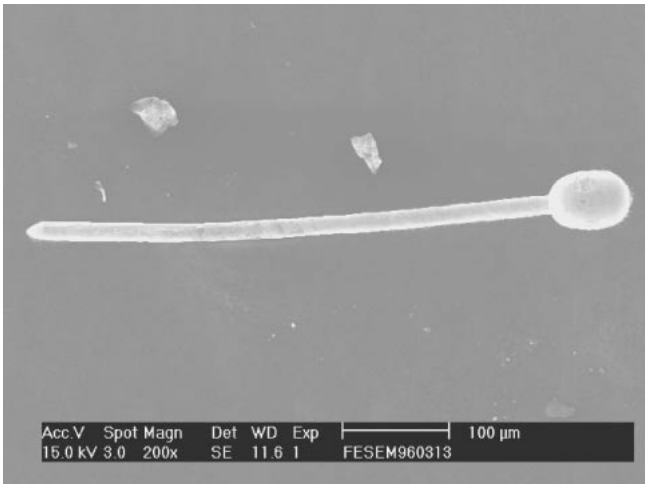

(b)

Fig. 6 Tensile fracture feature of the EFO wires (a) as-drawn EFO wire and (b) annealed EFO wire.

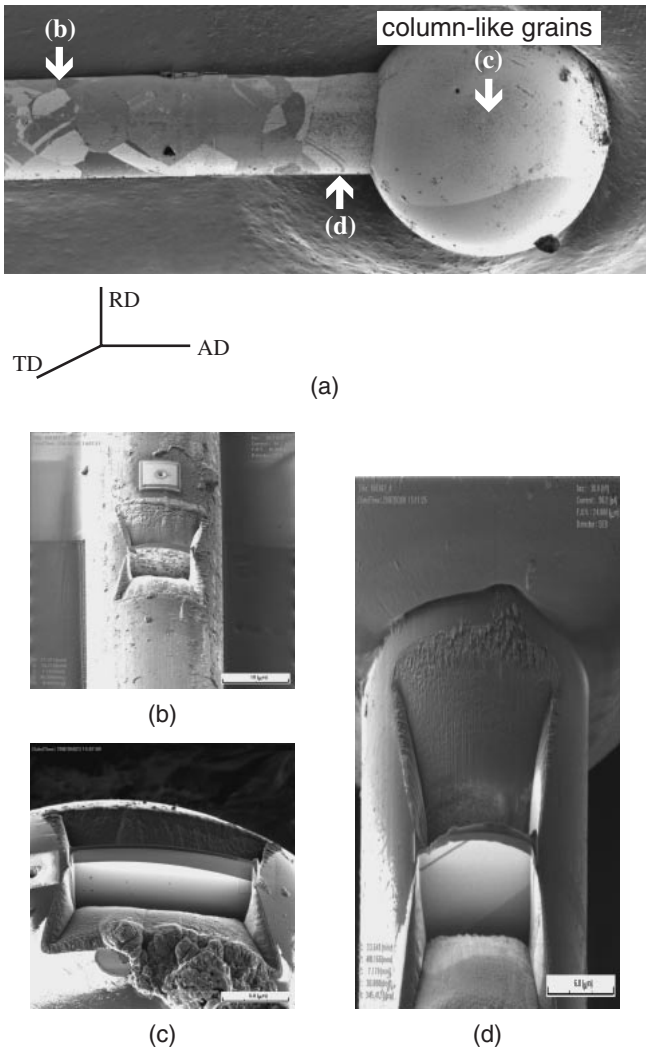

Fig. 7 EBSD positions of the annealed EFO wire: (a) SEM photo (b) wire (c) ball and (d) neck.

specimens, were drawn up using FIB to prepare the EBSD specimens, as shown in Fig. 7(b)(c)(d). In addition to the isotropic column-like grains, we also found that the necks of the Cu balls underwent grain regrowth during the EFO process. Through this EFO effect, the matrix structure transferred from its original fine equiaxed grains to large equiaxed grains and a few annealed twins.

In fact, the microstructure of the wire after the electric flame-off (EFO) can be divided into a solidification zone (i.e., the copper balls), a heat-affected zone (HAZ) induced by the EFO, and an unaffected zone. Figure 7(a) shows that continuous interfaces with no voids were found between the ball and the heat affected zone. So, it is safe to say that the column-like grains of the ball grew from the HAZ (i.e., the without-solidification wire) to the melting ball. Notably, all the Cu balls first melted then became solidified zones, their deformation behavior being closely related to the grain size and texture of the isotropic column-like grains. So, it was observed that the appearance of the Cu balls of the annealed wire after tensile testing looked like an ellipse, however the Cu ball of the un-annealed wire was still a round (Fig. 6). In addition, the hardness of the Cu balls and the crystallographic texture of the wires would determine the reliability of bonding.[3,6,9] For this reason, the texture characteristics of the Cu bonding wires still need to be examined.

Inverse pole figure (IPF) maps of the annealed wire,[15] including the wire, the neck and ball, were compared, as shown in Fig. 8–Fig. 10. The directions of AD, TD and RD follow the coordinate axes in Fig. 7(a). For the annealed and un-annealed wires, the preferred orientation on the wire or the neck were mostly ⟨100⟩ // AD and the orientation of the Cu balls was mainly ⟨101⟩ // AD and ⟨111⟩ // AD. The evidence confirms that the preferred orientations of the isotropic column-like grains were ⟨101⟩ and ⟨111⟩. Comparing the IPF data of Fig. 8 with Fig. 9, the orientations of the wires and the necks were mostly ⟨100⟩. Notably, some data of the neck-positions showed dispersion. This is because the neck-grains had grown during the EFO process. According to Fig. 4 and Fig. 6, the breakage site of the EFO wires was probably in the HAZ. The lengths of HAZ of the annealed wires were less than those of the as-drawn wires. So, it can be inferred that the 225°C annealing treatment not only

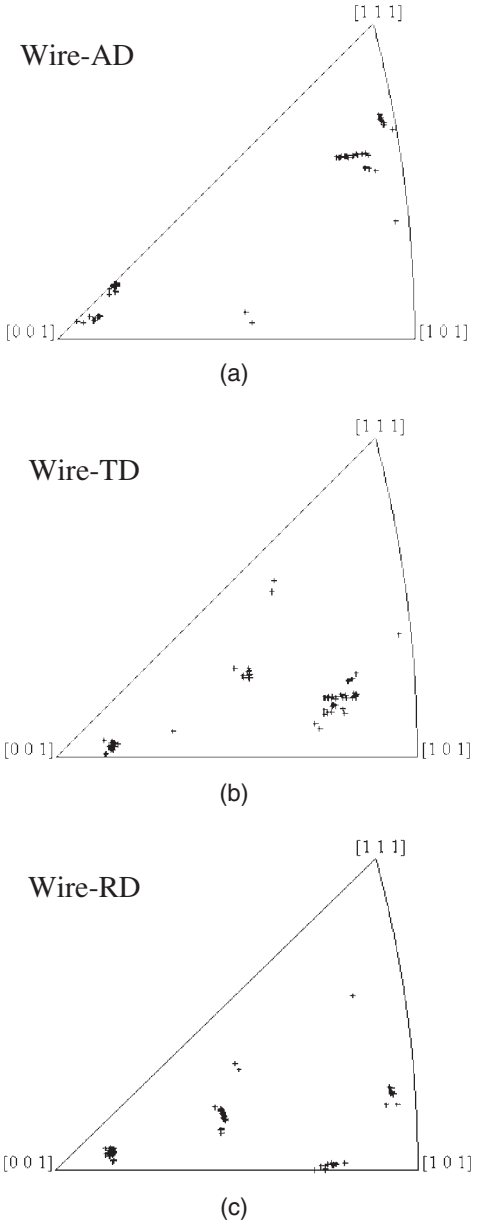

Fig. 8 IPF map of annealed wire: (a) AD, (b) TD and (c) RD.

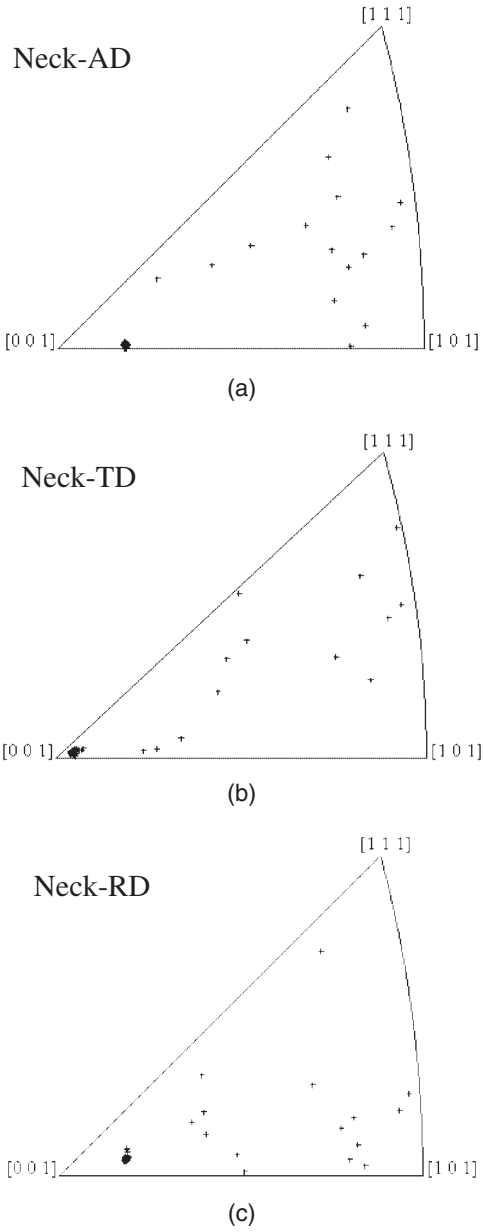

Fig. 9 IPF map of annealed wire on the neck: (a) AD, (b) TD and (c) RD.

shortened the length of HAZ, but also dispersed the texture of some grains at neck-positions. This is one reason why the breakage sites occurred within HAZ, not in the neck (near ball).

In addition, the IPF maps of the Cu balls are given in AD, TD and RD. The preferred orientation of both the annealed wires and non annealed wires were compared, as shown in Fig. 10 and Fig. 11. According to Fig. 10, an oriented grain growth mainly in ⟨101⟩ and ⟨111⟩ directions is observed. In Fig. 11, the grains are strongly oriented in ⟨100⟩ and ⟨101⟩ directions. Notably, the Cu ball of the annealed wire (Fig. 10) also had a predominant ⟨111⟩ texture component, which determined whether the deformation resistance of the Cu ball was low or high (Fig. 6). In other words, the ductility of the solidification ball possessed a stress relaxation effect, and the crystallographic texture of the column-like grain was able to affect the reliability of bonding.

4. Conclusions

(1) The recrystallization temperature of the 20 μm un-annealed wire was ∼225°C. The annealed wires contained fully annealed equiaxed grains with a few annealed twins. The breakage sites of the EFO wires were at the back of the neck, and the ductility of the Cu ball of the annealed wire was better than as-drawn wire.

(2) After the electric flame-off (EFO), the microstructure of the wire could be divided into a solidification copper ball, a HAZ induced by the EFO, and an unaffected zone. For the annealed and un-annealed wires, the orientations of the wires and the necks were mainly ⟨100⟩ // AD. For the annealed wires, the preferred orientation of the isotropic column-like grains in the Cu ball were ⟨101⟩ and ⟨111⟩.

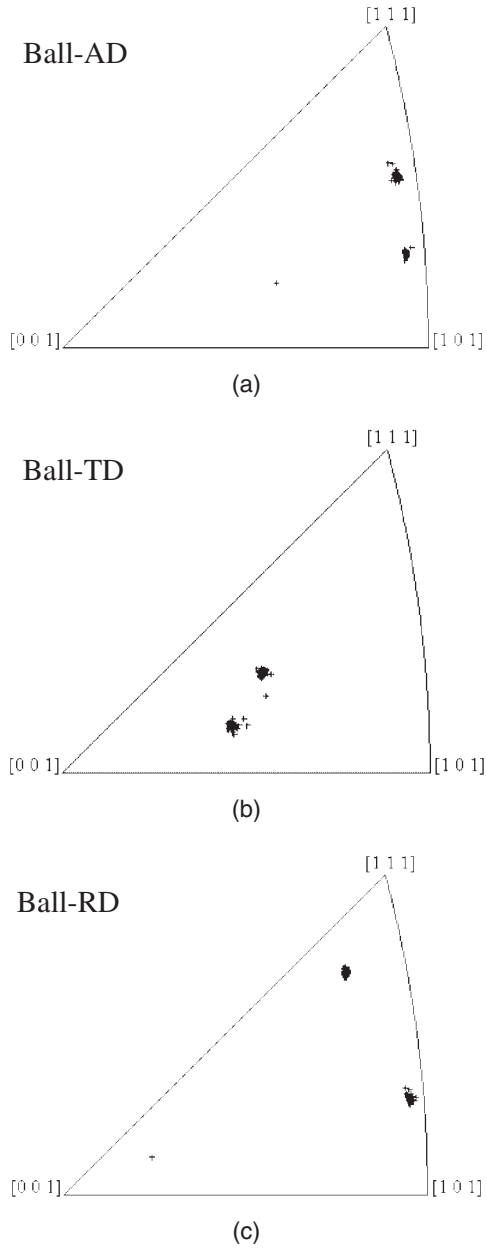

Fig. 10 IPF map of annealed wire on the ball: (a) AD, (b) TD and (c) RD.

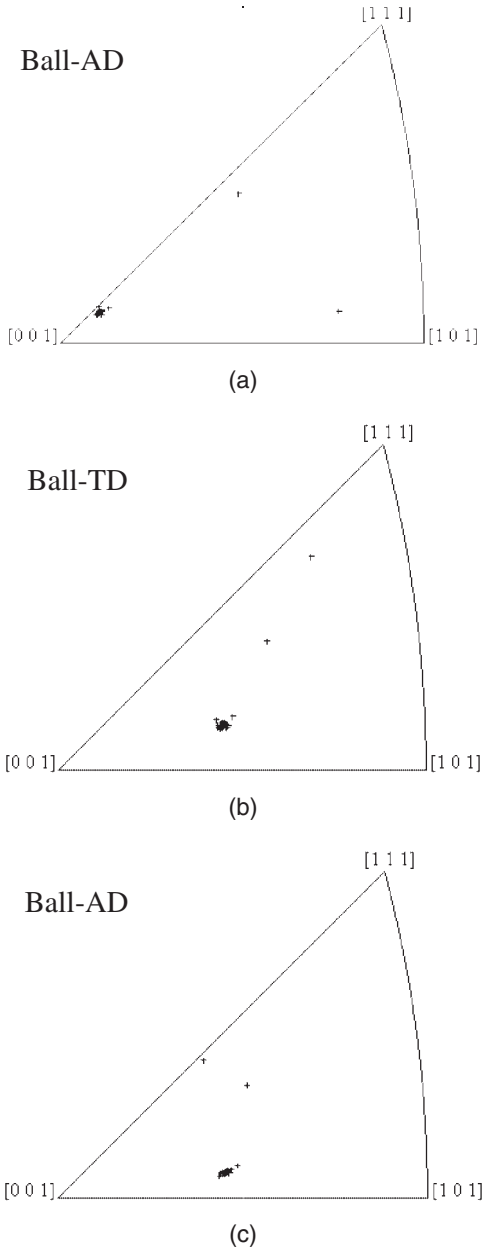

Fig. 11 IPF map of un-annealed wire on the ball: (a) AD, (b) TD and (c) RD.

Acknowledgements

The authors are grateful to National Cheng Kung University, the Center for Micro/Nano Science and Technology (D97-2700) and the Chinese National Science Council for its financial support (NSC 97-2221-E-006-018).

REFERENCES

1) F. Wulff, C. D. Breach and K. Dittmer: J. Mater. Sci. Lett. **22** (2003) 1373–1376.
2) N. Murali, N. Srikanth and C. J. Vath III: Mater. Res. Bull. **38** (2003) 637–646.
3) N. Srikanth, S. Murali, Y. M. Wong and C. J. Vath III: Thin Solid Films **462** (2004) 339–345.
4) *Properties and Selection: Nonferrous Alloys and Pure Metals, Metals Handbook*, Ninth Edition, Volume 2.
5) H. M. Ho, W. Lam, S. Stoukatch, P. Ratchev, C. J. Vath III and E. Beyne: Microelectron. Reliab. **43** (2003) 912–923.
6) S. Murali, N. Srikanth and C. J. Vath III: Mater. Charact. **50** (2003) 39–50.
7) A. Saboui: IEEE/CHMT IEMT Symposium, (1991) pp. 75–79.
8) F. Y. Hung, T. S. Lui, L. H. Chen and Y. T. Wang: J. Mater. Sci. **42** (2007) 5476–5482.
9) S. Jakani, T. Baudin, C. H. de Novion and M. H. Mathon: Mater. Sci. Eng. A **456** (2007) 261–269.
10) P. Ratchev, S. Stoukatch and B. Swinnen: Microelectron. Reliab. **46** (2006) 1315–1325.
11) F. Wulff, C. D. Breach and K. Dittmer: J. Mater. Sci. Lett. **22** (2003) 1373–1376.
12) M. R. Koblischka and A. Koblischka-Veneva: Phys. C **392–396** (2003) 545–556.
13) Z. W. Zhong, H. M. Ho, Y. C. Tan, W. C. Tan, H. M. Goh, B. H. Toh and J. Tan: Microelectron. Eng. **84** (2007) 368–374.
14) S. Murali, N. Srikanth and C. J. Vath III: Microelectron. Reliab. **46** (2006) 467–475.
15) F. Wullf, C. D. Breach and K. Dittmer: J. Mater. Sci. Lett. **22** (2003) 1373–1376.